

Polychaete-Like Undulatory Robotic Locomotion in Unstructured Substrates

Giovanni La Spina, Michael Sfakiotakis, Dimitris P. Tsakiris, *Member, IEEE*,
Arianna Menciassi, *Member, IEEE*, and Paolo Dario, *Fellow, IEEE*

Abstract—A biological paradigm of versatile locomotion and effective motion control is provided by the polychaete annelid worms, whose motion adapts to a large variety of unstructured environmental conditions (sand, mud, sediment, water, etc.), and could, thus, be of interest to replicate by robotic analogs. Their locomotion is characterized by the combination of a unique form of tail-to-head body undulations (opposite to snakes and eels), with the rowing-like action of numerous lateral appendages distributed along their long segmented body. Focusing on the former aspect of polychaete locomotion, computational models of crawling and swimming by such tail-to-head body undulations have been developed in this paper. These are based on the Lagrangian dynamics of the system and on resistive models of its interaction with the environment, and are used for simulation studies demonstrating the generation of undulatory gaits. Several biomimetic robotic prototypes have been developed, whose undulatory actuation achieves propulsion on sand and other granular unstructured environments. Extensive experimental studies demonstrate the feasibility of robot propulsion by tail-to-head body undulations in such environments, as well as the agreement of its qualitative and quantitative characteristics to the predictions of the corresponding computational models.

Index Terms—Biomimetic robotics, motion control, polychaete annelids, undulatory locomotion.

I. INTRODUCTION

LOCOMOTION and motion control are among the most significant problems for emerging robotic applications dealing with unstructured and tortuous environments; such applications range from novel diagnostic systems for healthcare (e.g., endoscopic access to the human body) to robotic tools for search-and-rescue operations and to planetary exploration. The human gastrointestinal tract, an earthquake-damaged building, or the Martian surface are environments quite different from the usual indoors environments, where most current mobile robots operate, and present significant challenges for locomotion. Drawing inspiration from biology, where such problems

Manuscript received August 31, 2006; revised May 10, 2007. This paper was recommended for publication by Associate Editor E. Papadopoulos and Editor F. Park upon evaluation of the reviewers' comments. This work was supported in part by the European Commission under Grant IST-2001-34181 through the IST Project BIOLOCH and under Grant FP6-033970 through the IST Project VECTOR. This paper was presented in part at the IEEE International Conference on Robotics and Automation, Barcelona, Spain, 2005.

G. La Spina, A. Menciassi, and P. Dario are with the Center for Research in Microengineering (CRIM) Laboratory, Scuola Superiore Sant'Anna, Pisa 56127, Italy (e-mail: giannilaspina@crim.ssup.it; arianna@sssup.it; dario@sssup.it).

M. Sfakiotakis and D. P. Tsakiris are with the Institute of Computer Science, Foundation for Research and Technology Hellas (FORTH), Heraklion 71110, Greece (e-mail: sfakios@ics.forth.gr; tsakiris@ics.forth.gr).

Color versions of one or more of the figures in this paper are available online at <http://ieeexplore.ieee.org>.

Digital Object Identifier 10.1109/TRO.2007.909791



Fig. 1. *Nereis virens* polychaete worm, crawling on the seashore sand as it emerges from the water. Photograph by Peter DeWit [19].

have been efficiently addressed by the evolutionary process, can help the design of agile robots, which are able to adapt robustly to a variety of environmental conditions; the study of lower animal forms (invertebrates, lower vertebrates), in particular, is inspiring robotic locomotion and the associated motion control strategies [1]–[8].

More specifically, undulatory locomotion is employed by a significant number of organisms, spanning a broad range of body sizes and environmental habitats, since it constitutes a satisfactory propulsion mechanism over a wide Reynolds number regime [9]. Particular attention has been devoted by robotics researchers to snake- and eel-like locomotion, leading mostly to wheeled mechanisms for terrestrial locomotion on relatively smooth surfaces (see [2], [10]–[13], and references therein), where propulsion is by lateral body waves propagating from the anterior to the posterior of the mechanism (head-to-tail body waves). The use of wheels in undulatory robots improves their efficiency on smooth surfaces, but fails to fully explore the key potential of terrain adaptability for this locomotion method. Recent research efforts on nonwheeled undulatory locomotion bring forth the importance of understanding the interaction of the undulatory mechanism with the environment enabling the locomotion [10], [14]–[18].

An intriguing biological paradigm of locomotion in unstructured environments is offered by a class of segmented marine worms, the polychaete annelids: these animals can be found swimming and crawling in the depths of the ocean, floating free near the surface, or burrowing in the mud and sand of the seashore (Fig. 1). The variety of their morphology, sensory apparatus, and nervous system structure is a direct consequence of their adaptation to so diverse habitats. Their locomotion, in particular, is characterized by the combination of a unique form of tail-to-head body undulations (opposite direction of propagation than snakes or eels), with the rowing-like action of the numerous active lateral appendages, called *parapodia*, distributed along

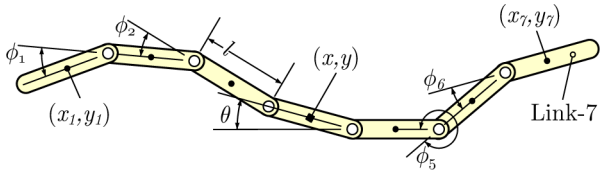


Fig. 2. Computational model of a 7-link undulatory mechanism.

their body [20]–[23]. Both characteristics provide these worms with distinctive locomotory modes, thus increasing their terrain traversing and manipulation capabilities and could benefit, if properly replicated, a robotic system [17], [18], [24]–[26].

The present paper focuses on the former aspect of polychaete locomotion, i.e., on obtaining propulsion by tail-to-head body waves. In doing so, we adopt the terms *polychaete-like* and *eel-like* for undulatory locomotion by tail-to-head and head-to-tail body waves, respectively. Section II provides models of the mechanics and motion control of undulatory robotic locomotors, focusing on the mechanism’s interaction with the locomotion environment. Associated simulation studies, employing the SIMUUN computational toolbox [27], are presented in Section III, and illustrate the generation of polychaete-like undulatory gaits, the conditions under which they are obtained, and their characteristics. A series of undulatory robotic prototypes, presented in Section IV, has been developed to investigate wheelless locomotion over sand and other unstructured environments, and to allow the validation and refinement of the computational models. The experimental setup utilized is described in Section V. Section VI presents the experiments performed with these prototypes, over three kinds of granular substrates, demonstrating the generation of polychaete-like undulatory gaits. The comparison between the experimental results and the ones obtained in simulation verifies their close agreement, ascertaining that the developed computational models capture adequately the main features of undulatory locomotion by tail-to-head body waves.

II. MODELING POLYCHAETE LOCOMOTION

A. Equations of Motion

The equations of motion of an undulatory robotic mechanism are obtained from its Lagrangian dynamics, after the *reduction* process described in [12], [28]–[32] and briefly outlined here. A computational model of a planar undulatory mechanism has been developed, based on a serial kinematic chain of N rigid links interconnected by planar revolute joints (we consider N odd; the case of $N = 7$ is shown in Fig. 2). The links are considered to be identical, with the center of mass of each link located at its geometrical center. Each of the $N - 1$ joint angles is considered to be independently actuated, to control the shape of the mechanism.

The position (x, y) and orientation θ of the central link with respect to an inertial coordinate frame on the plane are the system’s *group variables* and can be represented by an element g of the group $G = SE(2)$, the Special Euclidean group of order 2. The Lie algebra element, corresponding to g , is $\xi \triangleq$

$g^{-1}\dot{g} \in \mathcal{G} = se(2)$ and describes the *body velocity* of the central link. The joint angle vector $r = (\phi_1, \dots, \phi_{N-1}) \in \mathcal{S} \triangleq S^{N-1}$ denotes the *shape variables*, \mathcal{S} the *shape space* of the system and S the circle group. From the kinematics of the serial chain, it can be derived that the configuration of the mechanism is $q = (g, r) \in Q = G \times \mathcal{S} \triangleq SE(2) \times S^{N-1}$.

The Euler–Lagrange equations of motion can be reduced by exploiting the invariance of the mechanism to changes in inertial position and orientation, expressed as *Lie group symmetries* exhibited by the system. Assuming the existence of a Lagrangian function $\mathcal{L} : TQ \rightarrow \mathbb{R}$ and of external forces $F : TQ \rightarrow T^*Q$ acting on the system, both of which are invariant under the action of the group G , a reduced Lagrangian ℓ can be determined, which is a function of (r, \dot{r}, ξ) and takes the following form in body coordinates:

$$\ell(r, \dot{r}, \xi) = \frac{1}{2} \begin{pmatrix} \xi^T & \dot{r}^T \end{pmatrix} \begin{pmatrix} \mathbf{I}(r) & \mathbf{I}(r)\mathbf{A}(r) \\ \mathbf{A}^T(r)\mathbf{I}(r) & m(r) \end{pmatrix} \begin{pmatrix} \xi^T \\ \dot{r}^T \end{pmatrix}. \quad (1)$$

The matrix $\mathbf{A}(r)$ is the local form of the *mechanical connection*, and depends only on the shape r . The *local locked inertia tensor* $\mathbf{I}(r)$ describes the total inertia of the system, when all joints are frozen at a specific shape configuration r . The reduced equations of motion are, then, obtained in a body-fixed coordinate frame as:

$$\begin{aligned} \dot{g} &= g(-\mathbf{A}(r)\dot{r} + \mathbf{I}^{-1}(r)p) \\ \dot{p} &= ad_\xi^* p + f_T + f_N \\ \tilde{M}(r)\ddot{r} + \dot{r}^T \tilde{C}(r)\dot{r} + \tilde{N} &= B(r)\tau \end{aligned} \quad (2)$$

where p is the body momentum, defined as $p \triangleq \partial\ell/\partial\xi$; the reduced matrices $\tilde{M}, \tilde{C}, \tilde{N}$ are detailed in [32]; ad is the infinitesimal generator of the adjoint action of G on \mathcal{G} ; f_T, f_N are the external frictional forces in the tangential and normal directions of the central link, related to F , as described in [32], and are obtained from the frictional force model employed as a function of the tangential and normal velocities of each link (see Section II-B). The second equation, considered previously, describes the evolution of momentum in body coordinates (not conserved in this coordinate frame) and is called the *momentum equation*. The third equation, considered previously, is a second-order differential equation describing the evolution of the shape variables, as a function of the joint torques τ . The assumption will be made (and investigated experimentally) that full control of the shape variables is possible; therefore, the *controls* of the system are not considered to be the joint torques, but the joint angles r themselves. The equations (2) are computationally efficient and well suited to controller development. They are also used to validate the equations of motion derived automatically by the Matlab-based SIMUUN computational tools outlined in Section III, as detailed in [27].

B. Interaction With the Environment

Locomotion of an undulating body results from the coupling of its internal shape changes to external motion constraints, usually due to external frictional forces applied through the

interaction with the locomotion environment and resisting the motion of body segments. Computational models to approximate the characteristics of this interaction, both for aquatic and for terrestrial locomotion, have been implemented. These are of a resistive nature, i.e., the force on each link depends on its velocity (rather than acceleration), and they all involve decoupled force components in the normal and tangential direction of the link's motion. Use of such force models dates back to the analysis of the undulatory swimming of elongate animals in [33], and variants of this approach have been applied to both aquatic and terrestrial locomotion (see, e.g., [13], [14], [16], [17], [27], [29], [34], and [35]).

For the simple case of *viscous* frictional interaction with the substrate, the tangential and normal components of the force applied to the i th link of the mechanism are proportional to the respective components v_T^i and v_N^i of the link's velocity

$$F_T^i = -c_T v_T^i \quad \text{and} \quad F_N^i = -c_N v_N^i \quad (3)$$

where c_T and c_N are the viscous friction coefficients in the tangential and normal directions, respectively. Alternatively, for the *Coulomb* friction model, the applied frictional force depends only on the direction of the link's velocity, rather than on its magnitude

$$F_T^i = -\mu_T mg \operatorname{sgn}(v_T^i) \quad \text{and} \quad F_N^i = -\mu_N mg \operatorname{sgn}(v_N^i) \quad (4)$$

where μ_T and μ_N are the Coulomb friction coefficients, m is the mass of the link and g is the constant of gravity.

The friction coefficients in these models play a key role in undulatory propulsion. In a terrestrial locomotion context, their values depend on the configuration of the contact surface (the underside) of the undulatory mechanism's links, as well as on the material properties of the substrate. More importantly, it is the ratio of the friction coefficients, which, to a large extent, determines the stride length (distance traveled per undulation cycle) for a given body wave, as well as the overall motion direction of the undulatory locomotor with respect to the direction of the wave.

This is best illustrated in the context of propulsion by planar flagellar undulations in microorganisms, where the Reynolds number Re is of the order of 10^{-4} and the viscous force model can be used to approximate the fluid forces acting on the flagellum body. Such an approach facilitates the analytical treatment of the undulatory system (see [36]–[38], where a sinusoidal shape is assumed for the body wave), elucidating the effect of the friction coefficients c_T and c_N on the motion of the system. More specifically, it is established by the viscous force analysis that, when $c_T/c_N < 1$ (resp. $c_T/c_N > 1$), the overall motion of the undulatory system is in the direction opposite to (resp. same as) the propagation direction of the body wave. Indeed, the body of flagella, which propel themselves forward by head-to-tail body undulations is typically smooth, and, hence, the coefficient of normal resistance is greater than the coefficient of tangential resistance. By contrast, the surface of hispid flagella, which propel themselves forward by tail-to-head body undulations, is not smooth, but bears rigid, laterally protruding hair-like structures (called mastigonemes), by virtue of which the tangential friction coefficient is greater than the normal fric-

tion coefficient. It is worth noting that these findings have also been confirmed by computational fluid dynamics studies, which consider the 2-D full incompressible Navier–Stokes equations of low- Re flagellar propulsion [39]. Two additional predictions of this theoretical approach are of interest for the analysis of undulatory mechanisms with the viscous force model: 1) the magnitude of the propulsion speed increases with the *differential* between c_T and c_N (defined as the ratio of the friction coefficient with the greater magnitude over the coefficient with the lesser magnitude) and 2) in the case of uniform viscous friction (i.e., for $c_T/c_N = 1$), the undulatory movements of the body generate no net propulsive force and the system merely performs in-place undulations. We have been able to reproduce all of these findings with our computational models for undulatory mechanisms, where the links' interaction with the environment is described using the viscous force model (3), as detailed in Section III-B.

Similar conclusions, regarding the effect of body roughness (i.e., of the relative magnitude of normal/tangential frictional forces) on the overall locomotion direction of undulatory swimming animals, are reached in [33], which employs an alternate hydrodynamic model, applicable to a Reynolds regime of $Re > 1$ (for which the viscous force model is not suitable). Relevant examples of undulatory swimming organisms, to which this analysis may be applied, include eels (whose body is smooth and, ensuigly, propel themselves by head-to-tail body waves) and polychaete worms, the bodies of which afford a significant amount of roughness, mainly due to their parapodia, and, thus, propel themselves by tail-to-head waves [9], [33]. Note that, unlike the mastigonemes in hispid flagella, which remain rigid yet passive during the body undulations, the polychaete parapodia are active and exhibit wave-like rowing motions (cf. Fig. 1), which further contribute to the propulsive forces [20], [22]. This type of motion and the locomotory contributions of parapodia are not covered by the force models considered here, which only encapsulate the effect of the body undulations (see [18] for a study of parapodial forces in a polychaete-inspired robotic prototype).

In a robotics context, the viscous force model of (3) renders the analysis of the dynamics of undulatory mechanisms more tractable and, as such, has been used as a first approximation of the fluid drag forces for aquatic undulatory propulsion (see, e.g., [16] and [29]). For terrestrial undulatory robotic locomotion, a number of previous research efforts have employed variants of the Coulomb friction model to describe the interaction of the mechanism with the substrate (see, e.g., [13]–[15]), and this was also found to be the case for our robotic prototypes (see Section V). Although the general observations, made for the viscous friction model earlier, are also valid when Coulomb friction (4) is used, the effect of the Coulomb friction coefficients μ_T and μ_N on the locomotion characteristics is more complex in this case, while an analytical treatment of the system is significantly more involved. An illustrative example, which is also pertinent to our robotic prototypes, is the case $\mu_T/\mu_N = 1$, which typically results in the system moving in the same direction as the propulsive wave, rather than performing in-place undulations, as is the case for the viscous force model. A relevant investigation by simulations is provided in Section III-B.

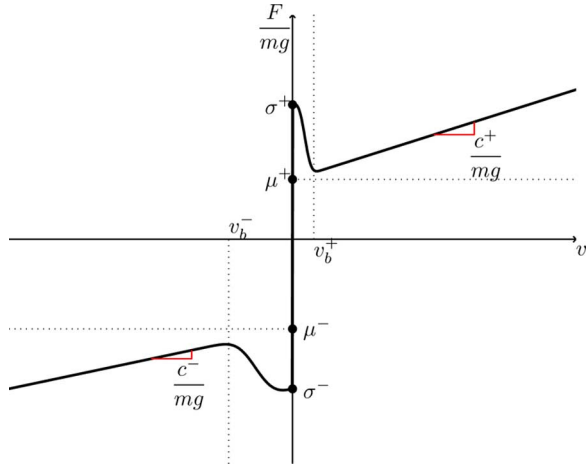


Fig. 3. General friction model, used for terrestrial locomotion.

In our robotic prototypes, the interaction of the mechanism's links with the substrate is via detachable segment contact modules (SCMs), which provide a friction differential in the tangential and normal directions of motion. For movement over relatively smooth surfaces, modules with passive wheels may be used, mounted either longitudinally or transversely with respect to the link's axis, in order to yield eel-like or polychaete-like locomotion, respectively. For movement over granular environments, such as sand, gravel, and mud, blade-bearing SCMs have been developed; these are described in Sections IV and V.

Finally, in order to allow coverage of the wider range of tribological phenomena encountered in different terrestrial substrates, a general friction model has been incorporated in the SIMUUN computational tools (outlined in Section III), which combines stiction, Coulomb friction, and viscous damping, as well as the Stribeck effect, and enables the implementation of anisotropic characteristics. The friction force acting on a rigid body with mass m is obtained as

$$F(v) = -\text{sgn}(v)mg \left(\mu + \frac{c}{mg} |v| + (\sigma - \mu)e^{-|3v/2v_b|^3} \right) \quad (5)$$

where σ and μ are the static and dynamic friction coefficients, respectively, c is the viscous damping coefficient, and v_b is the break-away velocity (described in [40]). To incorporate anisotropic friction, these parameters may assume different values for positive and negative values of v , as illustrated in Fig. 3. A total of 16 parameters are, then, required to fully describe the interaction with the environment for each link (eight parameters for the tangential and eight parameters for the normal directions of link movement).

C. Motion Control and Gait Generation

A straightforward way to explicitly generate a traveling wave in a serial chain of N links (Fig. 2), which has been extensively utilized in studies of undulatory locomotion (see, e.g., [2], [11]–[14], and [16]), is by having the $N - 1$ revolute joint angles vary sinusoidally, with a common amplitude A , frequency f , angular offset ψ , and a constant phase lag ϕ_{lag} between consecutive joints. This approach implies full control

of the mechanism's joint angles, without consideration of the required torques, specifying the temporal variation of the i th joint angle as

$$\phi_i(t) = A \sin(2\pi ft + (N - i)\phi_{\text{lag}}) + \psi, \quad 1 \leq i < N. \quad (6)$$

This formulation propagates a wave along the mechanism's body, whose shape (assuming links of equal length) is a discrete approximation of the *serpentine curve*, introduced in [2] to analyze the undulatory locomotion of snakes. Depending on the type of interaction with the locomotion environment (cf. Section II-B), the generated body wave will, then, propel the mechanism either in the direction of propagation of the body wave (polychaete-like) or in the opposite direction (eel-like). The propagation direction of the body wave depends on the sign of the phase lag parameter, and is from link-1 to link- N for $\phi_{\text{lag}} > 0$; if this wave propagation direction results in forward motion, then reversing the ϕ_{lag} sign results in backward motion. The condition $\phi_{\text{lag}} = \pm 2\pi/N$ yields (exactly) one wavelength of the propulsive wave across the undulating body. The angular offset ψ in (6) provides a means for steering along curved paths, and is set to $\psi = 0$ for locomotion along a straight line (*forward gait*). If ψ is nonzero, the mechanism moves along a curved path (*turning gait*), clockwise or counterclockwise, depending on the sign of ψ , as well as on the propagation direction of the wave (the sign of ϕ_{lag}), and on the undulatory mode (eel-like or polychaete-like) resulting from the interaction with the environment.

We also consider two additional gaits for the undulatory mechanism, namely *parallel-parking* and *in-place rotation*, similar to those formulated for a swimming eel-like robot in [16]. They both involve the generation of two traveling waves, characterized by the same values for the A , f , and ϕ_{lag} parameters, which emanate from the center of the mechanism and propagate in opposite directions. More specifically, in-place rotation is achieved by

$$\begin{aligned} \phi_i(t) &= \begin{cases} A \sin(2\pi ft + (i - M)\phi_{\text{lag}}) - \psi, & 1 \leq i \leq M \\ A \sin(2\pi ft + (M + 1 - i)\phi_{\text{lag}}) + \psi, & M < i < N \end{cases} \end{aligned} \quad (7)$$

where $M = (N - 1)/2$ (for N odd) is the index of the central link. Similarly, the parallel-parking gait is obtained by

$$\begin{aligned} \phi_i(t) &= \begin{cases} A \sin(2\pi ft + (i - M)\phi_{\text{lag}}) + \psi, & 1 \leq i \leq M \\ A \sin(2\pi ft + (M + 1 - i)\phi_{\text{lag}}) + \psi, & M < i < N. \end{cases} \end{aligned} \quad (8)$$

Note that, in order for these control schemes to be able to generate the corresponding gaits, the magnitude of the angular offset for the two body waves must be $\psi \neq 0$; otherwise, no net movement for the system (rotational or translational, respectively) can occur.

An alternative, biomimetic neuromuscular motion control scheme, which is based on central pattern generators to

generate the body traveling wave via joint torque control, is outlined in [7].

III. SIMULATION RESULTS

This section presents simulation studies, which illustrate the characteristics of undulatory locomotion by tail-to-head body waves (polychaete-like), and highlight its differences from locomotion by head-to-tail body waves (eel-like).

The simulations are set up using the SIMUUN simulation environment [27], developed at ICS-FORTH, which is based on the SimMechanics physical modeling toolbox of Matlab/Simulink. SIMUUN provides libraries of “body segment” and “shape control” modules, which are connected to simulate the mechanics and control of planar articulated robots. The associated equations of motion for the thus constructed undulatory systems are, then, derived automatically and solved using an appropriate integration scheme from the ones provided in Simulink. These tools have been used to create a computational model of the 11-link robotic prototype presented in Section IV, where the mechanism’s links are modeled as 2-D rectangular plates (length = 35 mm, width = 22 mm, and mass $m = 33$ g), interconnected by a total of 10 planar rotary joints. The latter are actuated according to the control strategies outlined in Section II-C, in order to generate the various undulatory gaits.

A. Polychaete-Like Undulatory Gait Generation

A first series of simulations explores the characteristics of undulatory gaits by tail-to-head body waves, using the Coulomb friction model with stiction to describe the interaction of the mechanism’s links with the locomotion environment. This particular force model, along with the values of the associated parameters, are specified to reflect the experimental conditions of locomotion over fine sand for our robotic prototype, as these were obtained by the series of measurements described in Section V. More specifically, the parameters in (5) are set as $\{\mu_N = 0.73, \sigma_N = 1.08, c_N = 0\}$ and $\{\mu_T = 0.88, \sigma_T = 1.18, c_T = 0\}$ for the normal and tangential directions, respectively, while $m = 33$ g and $v_b = 1$ mm/s. The resultant velocity versus frictional force characteristics are shown in Fig. 12. The control laws of (6)–(8) are, then, employed to generate the forward and turning undulatory gaits with $\phi_{lag} = 2\pi/N$ rad (i.e., implementing one full wavelength of the traveling wave along the mechanism), as well as the in-place rotation and parallel-parking gaits. The associated results are summarized in Fig. 4. Polychaete-like undulatory trajectories present a number of characteristics differentiating them from the more widely studied eel-like ones. These include the sickle-like shape of the tail link’s trajectory in forward motion [Fig. 4(a)], as well as the fact that, during turning, the mean path of distal links has a distinct offset from the mean path traced by the middle link [Fig. 4(b)].

The effect of the joint amplitude A and joint frequency f on the locomotion of the undulatory mechanism is important for altering the mean heading speed. This effect can be characterized, for the forward gait, in terms of the stride length, and is

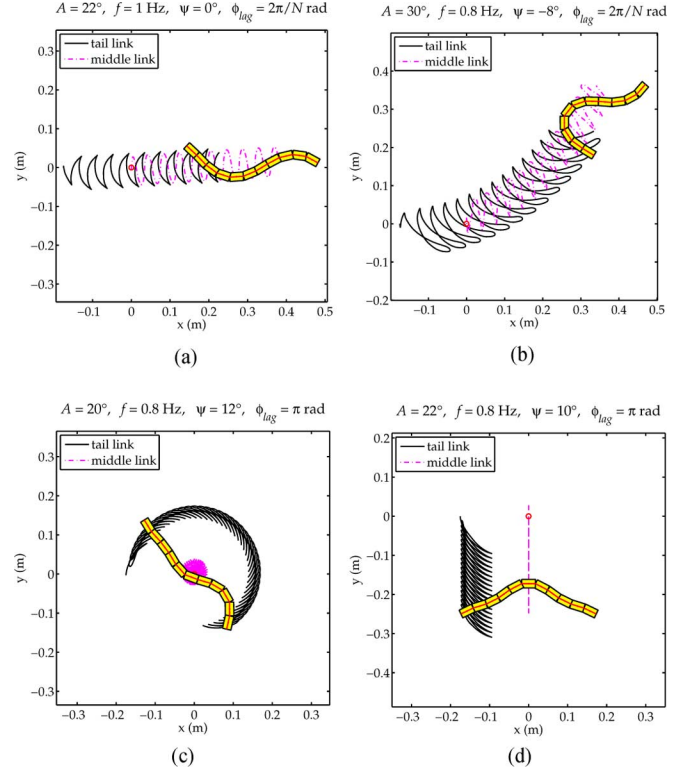


Fig. 4. Simulations of undulatory gaits for the 11-link prototype. At $t = 0$, the mechanism is aligned with the x -axis and the center of the middle link is located at point $(0, 0)$. (a) Forward gait. (b) Turning gait. (c) In-place rotation gait. (d) Parallel-parking gait.

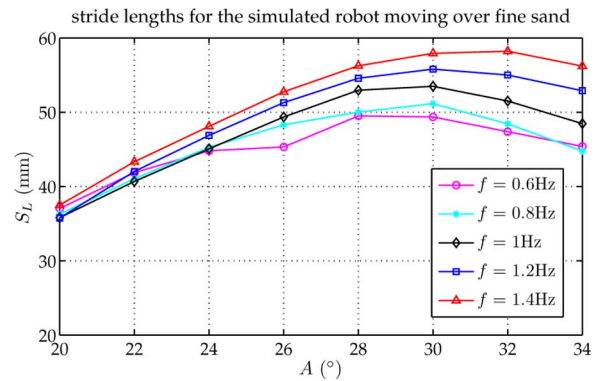


Fig. 5. Parametric study of stride length in simulation.

shown in Fig. 5 for a range of A and f values, which reflect the experimental conditions of our robotic prototypes.

B. Effect of Friction Coefficients on Forward Gait

A second series of simulations explores the effect of the friction coefficients on the efficiency of the propulsion, both for the polychaete-like and for the eel-like regimes. Two sets of parametric investigations have been carried out, one using the viscous force model of (3), and one using the Coulomb model of (4) for the interaction of the mechanism’s links with the locomotion environment; both sets have considered an extended range of values for the friction coefficients (c_T, c_N and μ_T, μ_N ,

respectively). Although the latter is the most relevant to our experiments, the viscous model simulations have been included in this paper in order to better highlight the differentiating characteristics of the system's behavior under Coulombian interaction with the environment.

1) *Viscous Friction*: Simulations of the forward undulatory gait with $f = 1$ Hz, $\phi_{lag} = 2\pi/N$ rad and for $10^\circ \leq A \leq 50^\circ$, are performed using the viscous force model, over the following ranges of the friction coefficients' ratio c_T/c_N : 1) for $1 \leq c_T/c_N \leq 4$, with $c_N = 0.22$ kg/s and 2) for $1/4 \leq c_T/c_N \leq 1$, with $c_T = 0.22$ kg/s. The rationale behind selecting such a scheme for the friction coefficients can be intuitively explained on the basis of the SCMs, like the ones developed for our robotic prototypes (see Sections IV and V and Fig. 10), whose morphology gives rise to a friction differential in the range 1–4, for an assumed locomotion environment. Depending on their mounting orientation with respect to the link's main axis, these can, then, yield greater resistance in either the tangential (case 1) earlier) or the normal (case 2) earlier) direction of link motion.

To assess the effect of the friction parameters and the joint oscillation amplitude on the propulsion efficiency, the following metrics are used (all of them are calculated from the steady-state response of the system, i.e., when its average acceleration is zero): 1) the *stride length* S_L , which represents the distance travelled per undulation cycle; 2) the *average total power expenditure* over one undulation period $T = 1/f$, which is $P \triangleq \frac{1}{T} \int_{t_0}^{t_0+T} \sum_{i=1}^{N-1} |\tau_i(t) \dot{\phi}_i(t)| dt$, where $\tau_i(t)$ and $\dot{\phi}_i(t)$ are the torque and angular velocity of the mechanism's i th joint, while t_0 specifies a time instance in the steady-state response of the system; and 3) the *locomotion efficiency* η , which is defined here as the inverse of the specific resistance [41], and is given by the nondimensional ratio $\eta \triangleq k S_L / P$, where the quantity $k \triangleq m N g / T$ remains constant in the current parametric study.

The corresponding results for the viscous friction model are summarized in Fig. 6. The stride length plots illustrate that, when $c_T/c_N > 1$, the mechanism moves in polychaete-like mode (i.e., its motion is along the direction of the body wave), designated by positive values for S_L (blue-colored region) in Fig. 6(a). In that case, the attained stride length is gradually reduced as the c_T/c_N ratio approaches 1. At the point of uniform friction (i.e., for $c_T/c_N = 1$), and irrespective of the joint oscillation amplitude A , the stride length becomes zero, i.e., the mechanism performs in-place undulations. Thereafter, for $c_T/c_N < 1$, the system moves in eel-like mode (i.e., its motion is in the direction opposite to that of the body wave), designated by negative values for S_L (red-colored region) in Fig. 6(a), with S_L increasing with the inverse of the c_T/c_N ratio. This behavior of the undulatory system is consistent with the predictions of the corresponding analytical models [36]–[38] outlined in Section II-B. It may also be observed that, for any given friction differential, and for values of A up to about 35° , consistently greater stride lengths are attained by the eel-like mode. As the amplitude of the joint oscillations is further increased, the stride lengths for the polychaete-like mode are comparable to or larger than the ones attained with the eel-like mode, but with considerably increased power expenditure. The plot in Fig. 6(b)

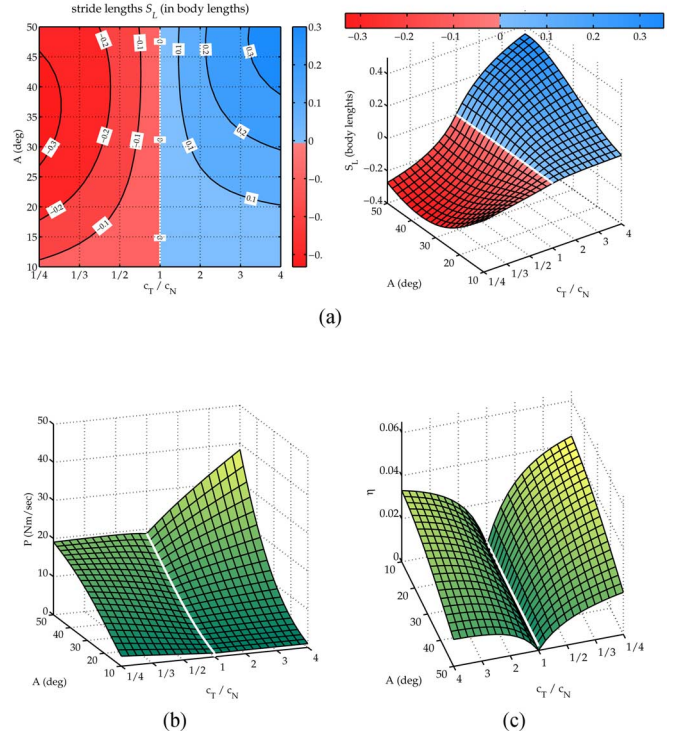


Fig. 6. Viscous friction model: Parametric study of polychaete-like and eel-like undulatory locomotion. The transition between the two regimes lies along the $S_L = 0$ line (white line overlaid in plots). For visualization purposes, the direction of the c_T/c_N -axis and of the A -axis in (c) is inverted with respect to the ones in (a) and (b). (a) Stride length: contour plot (left) and 3D plot (right). Modes of locomotion: eel-like (red) and polychaete-like (blue). (b) Power expenditure. (c) Locomotion efficiency.

further indicates that, for both regimes, the power requirements P increase as the friction differential or the joint oscillation amplitude are increased, while the eel-like mode is, in general, associated with smaller values of P . Moreover, uniform friction represents the case for which the two friction coefficients assume the minimum value in their range ($c_T = c_N = 0.22$), and is associated with the least power input requirements, for a specific value of A . As a consequence of these observations related to S_L and P , and as Fig. 6(c) demonstrates, propulsion by the eel-like mode is more efficient (higher values of η) than by the polychaete-like undulatory mode. Note that, for both regimes, η increases with the friction differential, but is decreasing with the joint oscillation amplitude A .

2) *Coulomb Friction*: Analogous simulations are carried out for the Coulomb model, using the same body wave parameters, and considering the same ranges for the μ_T/μ_N friction coefficients' ratio, as for the viscous force model, i.e.: 1) for $1 \leq \mu_T/\mu_N \leq 4$, with $\mu_N = 0.22$ and 2) for $1/4 \leq \mu_T/\mu_N \leq 1$, with $\mu_T = 0.22$ (note that, contrary to c_N and c_T , μ_T and μ_N are nondimensional). The corresponding results, summarized in Fig. 7, indicate that, to a large extent, the behavior of the undulatory system under Coulomb friction is similar to the one obtained under viscous friction. However, a number of important differences are identified: the stride length plots in Fig. 7(a) reveal that the transition from the eel-like mode (red-colored region) to the

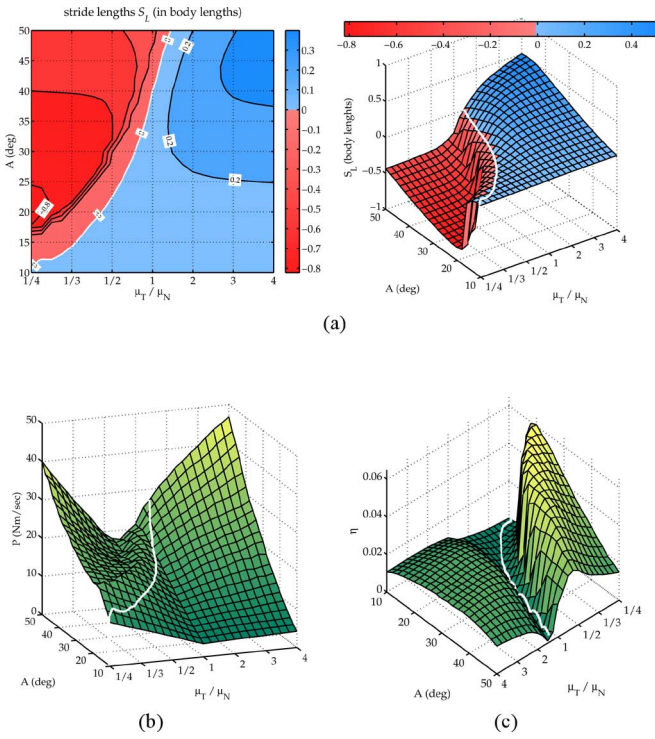


Fig. 7. Coulomb friction model: Parametric study of polychaete-like and eel-like undulatory locomotion. The transition between the two regimes lies along the $S_L = 0$ line (white line overlaid in plots). The direction of the μ_T / μ_N -axis and of the A -axis in (c) is inverted with respect to the ones in (a) and (b). (a) Stride length: contour plot (left) and 3D plot (right). Modes of locomotion: eel-like (red) and polychaete-like (blue). (b) Power expenditure. (c) Locomotion efficiency.

polychaete-like mode (blue-colored region) depends on both the μ_T / μ_N value and on A (and, possibly, on other characteristics of the mechanism, like its number of links N). Indeed, when the friction differential is around 1, or when the joint oscillation amplitude is low, the system can be seen to predominantly move in polychaete-like mode. Overall, however, the stride lengths attained in the eel-like regime are considerably higher for the parameter range considered in the simulations. These findings are consistent with the results reported in previous studies of undulatory mechanisms under Coulomb frictional forces [13]–[15]. Regarding the power requirements, the general trends identified for the viscous force model also hold for the Coulomb model [cf. Figs. 7(b) and 6(b)]. Finally, Fig. 7(c) indicates that, much like for the viscous model, the eel-like mode is characterized by higher locomotion efficiency η , than the polychaete-like mode.

C. Burrowing

Burrowing tasks are of particular interest for the intended applications of undulatory robotic locomotors. Biological evidence indicates that low-amplitude tail-to-head body waves assist the polychaete worms during the early phases of burrowing, which is a common activity among these animals [23]. Supposing that the “head” link (i.e., the link foremost with respect to the motion direction of the mechanism) plays the most significant role, among all links, in penetrating the substrate, data

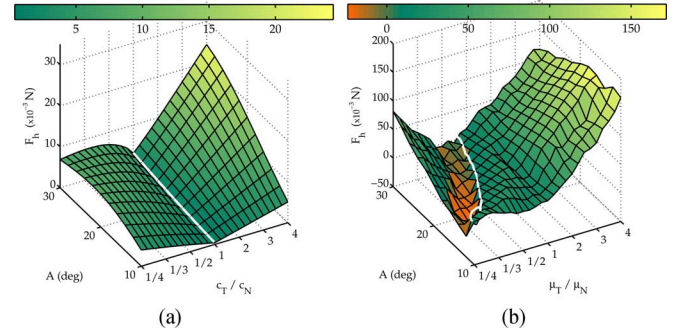


Fig. 8. Parametric study of the average head link force, for polychaete-like and eel-like undulatory locomotion (the transition between the two regimes lies along the white line, corresponding to $S_L = 0$, overlaid in the plots). In each case, positive F_h values indicate forces exerted in the direction of locomotion. (a) Viscous model. (b) Coulomb mode.

from the simulation series of Section III-B were used to estimate burrowing potential for the undulatory mechanism. This is characterized in terms of the average force F_h exerted by the head link along the mean direction of motion during the forward gait, for a range of joint oscillation amplitudes and friction coefficients’ ratios. The results, shown in Fig. 8, indicate that greater forces are, in general, generated on the head link, for both the viscous and the Coulomb force models, when forward undulatory locomotion is by tail-to-head body waves, compared to the case of head-to-tail body waves. This suggests that the polychaete-like mode may be more suitable for burrowing tasks than the eel-like one.

IV. UNDULATORY ROBOTIC PROTOTYPES

A series of robotic prototypes has been developed, using off-the-shelf components and traditional fabrication technologies, in order to experimentally investigate polychaete-like undulatory locomotion and to allow the assessment of the computational models described in the previous sections.

The first such prototype, shown in Fig. 9, was composed of $N = 8$ segments (link mass 42 g, length 47 mm, width 52 mm), which were fabricated from Delrin with aluminum interconnecting links. The seven rotary joints of the mechanism were actuated using *Hitec* HS-81 microservo motors, controlled by a *Microchip* PIC18F252 microcontroller. This first prototype successfully demonstrated, for the first time, forward and turning locomotion by tail-to-head body waves over fine sand. However, it presented a number of reliability issues, mainly due to the servos overheating and to the aluminum linkages’ susceptibility to braking, which prohibited carrying out extensive tests with it.

A second prototype, shown in Fig. 10(a), was developed in order to overcome these reliability issues. It is composed of $N = 11$ segments, which have been designed to be stronger, yet smaller and lighter (link mass 33 g, length 35 mm, width 22 mm) than the ones of the first prototype. The larger number of segments yields more accurate body waves and facilitates implementation of the more demanding parallel-parking and in-place-rotation gaits. The rotary joints are actuated by *Hype*

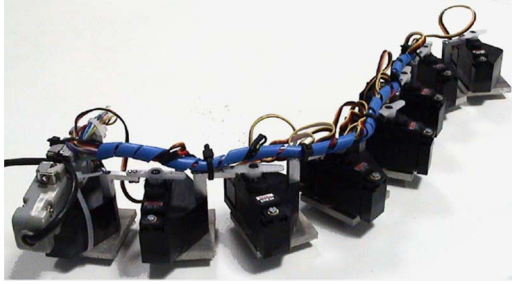


Fig. 9. Eight-segment undulatory robotic prototype.

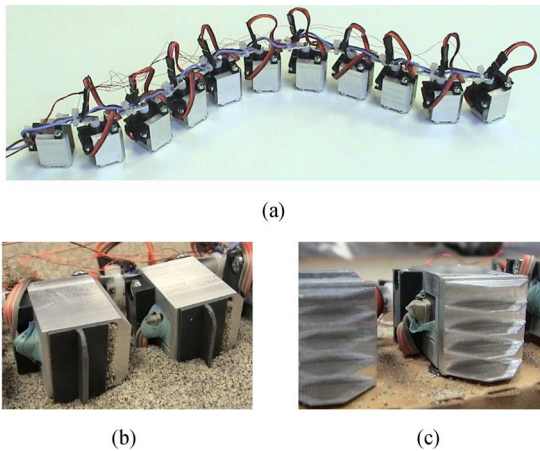


Fig. 10. (a) Eleven-segment undulatory robotic prototype without segment contact modules. (b) Single-blade SCM mounted transversely to the segment. (c) Multi-blade SCM, mounted longitudinally to the segment.

Mini 11s servos, while the aluminum servo frame used ensures effective heat dissipation during prolonged testing. The linkage between consecutive segments utilizes aluminum bridges, whose geometry has been designed to combine high bending flexibility with increased torsional stiffness. This facilitates adaptation of the robot shape to unstructured environments, without compromising the smoothness of the locomotory wave.

The interaction of the robot's segments with the granular locomotion substrate is via detachable SCMs, which employ blades for generating a frictional differential in the tangential and normal direction of motion. Two SCM designs have been developed and tested: the first one exploiting a single blade of Delrin, and the second one made of five aluminum blades. Both can be mounted either transversely or longitudinally with respect to the main axis of the segment, as shown in Fig. 10(b) and (c).

The servos are controlled by a *Pololu* serial 16-servo board, which receives the joints' angular trajectories from a host personal computer (PC) via an RS-232 connection. A Visual Basic program, running on the host PC, is used to generate the joint angle profiles for the undulatory gaits (forward, turning, in-place-rotation, and parallel-parking), where the amplitude, frequency, and phase offset are the main parameters, tunable via a graphical user interface (GUI).

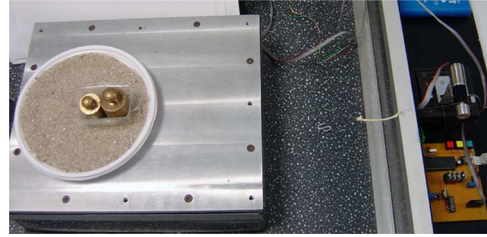


Fig. 11. Test-bed used for the SCM frictional force measurements.

TABLE I
DATA FROM THE SCM FRICTIONAL FORCE MEASUREMENTS

FINE SAND	Single-blade SCM		Multi-blade SCM	
		⊥		⊥
	Static friction coefficients			
	1.08	1.18	1.09	1.22
Traction velocity (mm / s)	Dynamic friction coefficients			
$v_1 = 5.8$	0.73	0.85	0.93	1.15
$v_2 = 8.0$	0.68	0.85	0.96	1.07
$v_3 = 11.0$	0.71	0.89	0.84	1.12
$v_4 = 13.4$	0.76	0.91	1.07	1.26
$v_5 = 18.2$	0.77	0.92	0.97	1.19
Mean	0.73	0.88	0.95	1.15

V. THE EXPERIMENTAL SETUP

This section describes the experimental setup utilized to test the capabilities of the 11-segment prototype for undulatory gait generation over unstructured environments and to assess the previously presented computational models.

In order to compare experimental and simulation results, data on the frictional characteristics of the mechanism are required, taking into account the configuration of the SCM used (i.e., single- or multiblade design and transversal or longitudinal SCM placement) and the specific locomotion substrate. Such data are used to select the appropriate force model for the SIMUUN simulations and to specify the numerical values of the associated parameters. A custom test-bed, shown in Fig. 11, has been constructed to obtain these data, utilizing a pulley, a motor, and a load cell to measure the required forces for moving the SCM along the locomotion substrate at different velocities.

The associated results, for SCM motion over fine sand, are summarized in Table I for single- and multiblade SCMs, when the blades are parallel (||) to the traction direction and when they are perpendicular (⊥) to it. Data on the table are expressed in terms of the measured frictional forces divided by mg , where m is the segment mass. The results indicate that the frictional forces for the multiblade SCM design, in both directions of motion, are higher in magnitude than those for the single-blade SCM design; however, the resulting friction differential for the two designs is almost the same (with a value of around 1.2). This suggests that employing the multiblade SCM in the robot will improve locomotion performance only slightly, while increasing the energy requirements for implementing the same body wave, compared to the single-blade SCM. This favors the use of the latter SCM type with the prototype.

The data of Table I indicate that, for both SCM designs, the frictional forces generated show a relatively small variance

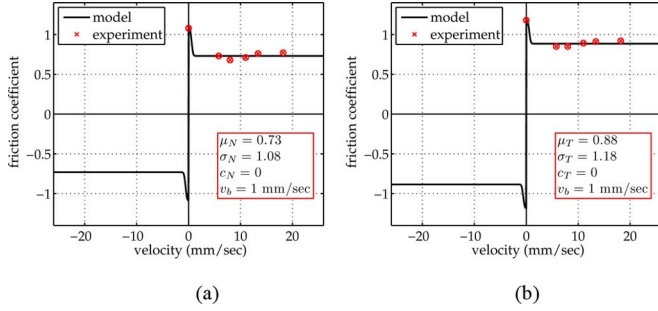


Fig. 12. Friction model employed in the SIMUUN simulations of the 11-link undulatory mechanism with the single-blade SCM design. (a) Normal force component. (b) Tangential force component.

with traction velocity. On the basis of this, a Coulomb friction model with stiction has been used to approximate the interaction of the robot with the sand. The resulting relationship between traction velocity and frictional force, obtained by appropriately specifying the parameters of (5), for the single-blade SCM on fine sand, is illustrated in Fig. 12.

In order to obtain polychaete-like conditions, where the tangential resistance to link motion is higher than the normal resistance, the SCM units are placed, following the results of Table I, so that their blades are transverse to the segment's main axis, both for single-blade [cf. Fig. 10(b)] and multiblade SCMs. With these experimental conditions, the perpendicular direction results (\perp) of Table I correspond to tangential friction, while the parallel ones (\parallel) to normal friction.

For the experiments, the prototype is placed inside a cardboard box (measuring 1 m \times 0.7 m), which is uniformly filled with 20 mm of each of the substrates tested (i.e., fine sand, coarse sand, and gravel), thus ensuring that, throughout the robot's movement, the SCM blades are never in contact with the bottom of the box. The motions of the robot are tracked using a 3-D optical motion analysis system (*Image Guided Technologies FlashPoint 5000*), which is able to simultaneously acquire in real-time the positions of several light spots (infrared emitters). A total of nine such infrared emitters are used with the robot, mounted on individual frames and placed over each of the mechanism's joints, in order to track their movements. The tracking head of the localizer is appropriately placed over the area of the experiments, to ensure its uniform coverage.

VI. EXPERIMENTAL RESULTS

The results of the experiments, investigating the generation of undulatory gaits over unstructured environments with the 11-segment robotic prototype, are presented here. Tests with the multiblade SCM units, indicated that the higher resistance forces associated with it (cf. Table I) hinder the robot's actuators from closely following the prescribed joint angle profiles. Therefore, most of the experiments have been performed with the single-blade SCM units mounted transversely on the underside of the segments, as indicated in Fig. 10(b), for which the aforementioned problem appeared only to a lesser extent.

Using this configuration, the control laws of Section II-C are implemented with the prototype moving over fine sand, coarse sand, and gravel, to produce, for each of these substrates, the four main undulatory gaits considered in this paper. In all cases, the motion of the robot is polychaete-like and the gaits exhibit the main characteristics identified in the equivalent simulation studies of Section III-A.

Representative results from experiments over fine sand (mean particle diameter 0.56 mm) are shown in Fig. 13, both in terms of pictures of the traces left by the robot as it moves on the sand (on the right) and in terms of trajectory plots generated from the 3-D localizer data (on the left). In Fig. 13(e) and (f), the robot moves from left to right (along the direction of the body wave) using the forward and turning gaits. The robot length in these pictures can be used as an indication of the travelled distance; this distance is shown explicitly on the links' trajectory plots of Fig. 13(a) and (b). Backward movement is obtained simply by reversing the body wave direction, i.e., by inverting the sign of ϕ_{lag} in (6). In Fig. 13(g), the robot rotates clockwise by more than π rad using the in-place rotation gait [trajectory plot in Fig. 13(c)]. In Fig. 13(h), the robot moves downward, laterally to its longitudinal axis, using the parallel-parking gait [trajectory plot in Fig. 13(d)].

Significant qualitative agreement can be observed between the robot link trajectory plots from the experiments (Fig. 13) and from the corresponding simulation results (Fig. 4). The sickle-like trajectory of the links seen in the forward gait [Fig. 13(a) and (e)] is similar to the one obtained in simulation [Fig. 4(a)]. In Fig. 13(e) and (f), the robot can be seen to dig a small trench, as it propels itself forward, while, simultaneously, displacing the sand (a form of burrowing). This is particularly pronounced during the turning gait [Fig. 13(f)], where, as mentioned in Section III-A, the paths of distal links have a relative offset [Fig. 13(b)]: the lower part of the trench seen in this picture is due to the tail link, while the upper part is due to the head.

Estimates of the stride lengths S_L , achieved by the robot during the forward gait experiments, are obtained by analyzing the associated trajectory data. The mean velocity for each experiment is, subsequently, estimated as fS_L , for the joint oscillation frequency f used. The results, summarized in Fig. 14, indicate that the robot achieves velocities in the range of 90–200 m/h, and confirm the simulation results of Fig. 14 indicating that higher velocities are associated with increased values for A and f . Furthermore, it can be seen that the simulation-derived velocities demonstrate close agreement with the experimentally obtained ones.

Regarding the other three gaits investigated on fine sand, it can be seen that they have been, in general, successfully implemented, as the robot's motions are qualitatively consistent with the ones predicted through simulations [cf. Fig. 4(b)–(d)]. However, there was comparatively greater discrepancy in their implementation, as the robot generally required a greater number of undulation cycles to perform movements equivalent to what the simulations predicted. This is exemplified by the turning gait trajectories shown in Figs. 4(b) and 13(b), where it can be seen that, in simulation, the mechanism requires 14 undulation

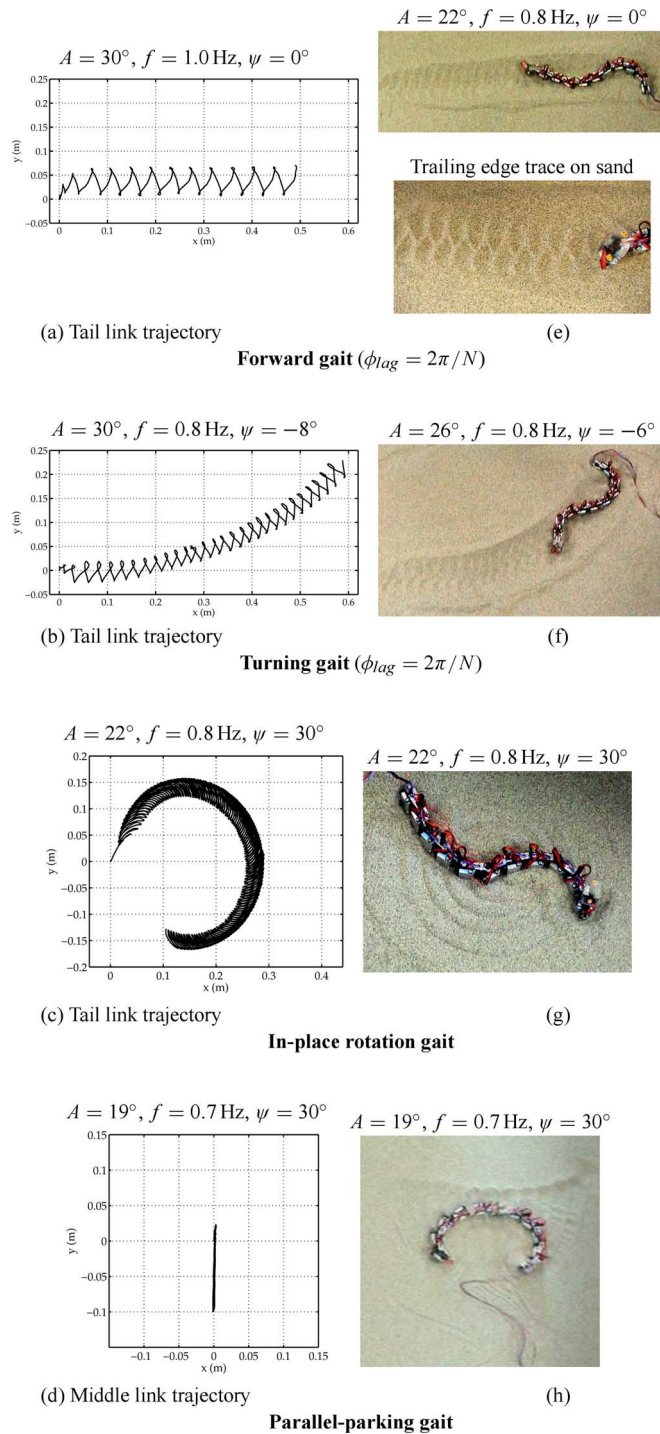


Fig. 13. Experimental results demonstrating polychaete-like undulatory gait generation on *fine sand* by the 11-link prototype: (a–d) Representative link trajectories, (e–h) Image stills. In all instances, the initial position of the robot is along the x -axis. The forward gait results presented earlier, were obtained with single-blade SCMs, while the rest involved multiblade SCMs.

cycles to perform an orientation change of about 45° (thus yielding a turning performance of approximately 3.2° per undulation cycle); by comparison, in the equivalent experiment, the robot performs an orientation change of about 45° within 28 undulation cycles, hence exhibiting a turning performance of 1.6° per undulation cycle. This results in a trajectory with a

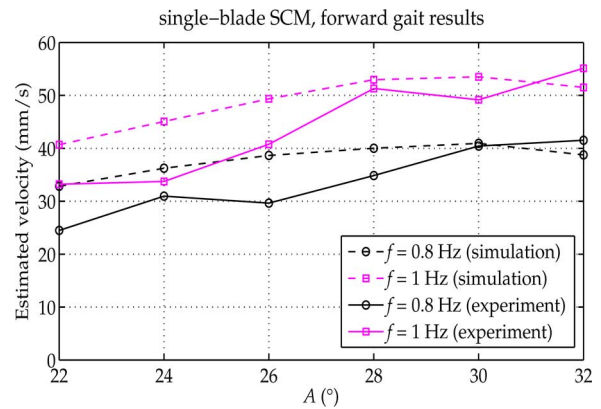


Fig. 14. Estimated velocities of the robotic prototype obtained from experiments (solid lines), compared with simulation results (dashed lines).

significantly increased turning radius compared to the simulation. Similar observations can be made for the in-place rotation and the parallel-parking gaits.

These discrepancies could be attributed, in part, to the friction model used in the simulations. Due to its simplified nature, it cannot describe the whole range of complex phenomena and interactions, tribological or otherwise (e.g., sand shifting or sand compaction by the blades), which take place between the robot's segments and the highly unstructured granular substrates considered in this experimental study. Such interactions are particularly prominent during the in-place rotation and parallel-parking gaits. It is noteworthy that the implementation of these two gaits in an aquatic environment, as reported in [16], is characterized by interactions with water of analogous complexity, which restrict the ability of computational models based on simple resistive friction forces (i.e., of a similar nature to the ones used here) to accurately predict (on a quantitative basis) the motion of the undulatory robot.

Another potential source for the discrepancies between the experimental and the simulation results lies in the use of R/C servo motors in the developed prototypes. Although this is a simple solution, providing straightforward position control for the joints' rotary movements, these motors provide no position feedback output; therefore, it is not possible to verify how accurately the prescribed joint angle profiles, and, hence, the prescribed body wave, are being reproduced in individual test runs. This was evident, particularly when multiblade SCMs were used, in experiments involving higher values for both A and f where the actuators were reaching their output torque limits, which typically led to the implementation of a body wave with reduced amplitude (the joint oscillation frequency was not significantly affected in these cases). The actuators were also under increased stress during the implementation of the more challenging in-place rotation and parallel-parking gaits, where, as described previously, significant sand-shifting occurs.

Despite these limitations, the overall results indicate that the computational models used in this paper are able to capture adequately the dominant characteristics of the robot's interaction with the environment and to predict the system's motion.

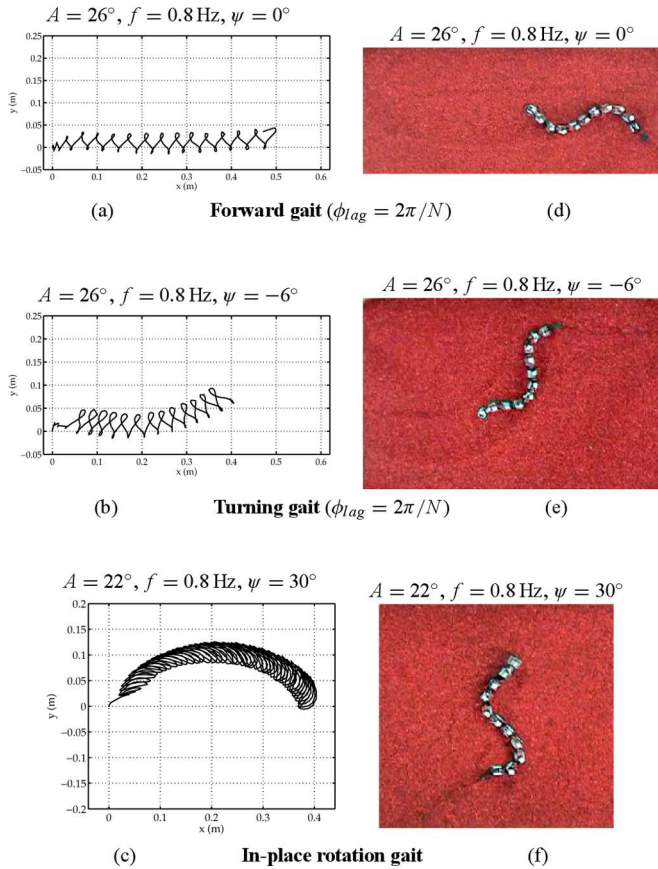


Fig. 15. Experimental results demonstrating polychaete-like undulatory gait generation on *coarse sand* by the 11-link prototype equipped with single-blade SCMs: (a–c) Representative trajectories of the mechanism’s tail link, (d–f) Image stills. In all instances, the robot initially lies along the x -axis.

During experiments involving coarse sand and gravel (mean particle diameters equal to 1.5 mm and 3.4 mm, respectively), the main undulatory gaits have also been successfully generated, although the increased complexity of the segments’ interaction with these environments has further affected their implementation. Comparing the corresponding results in Figs. 15 and 16 with those of Fig. 13, reveals that, as the mean particle diameter of the granular substrate increases from fine sand to gravel, the accuracy with which the gaits are implemented and the repeatability of the obtained movements both decline. This is evident in, e.g., the forward gait trajectories, where the variance of the movement stride, for different undulation cycles, even throughout a single test run, is increasing as the substrate is changed from fine sand, to coarse sand and gravel.

The tests carried out with the 11-link robotic prototype have verified the viability of employing the polychaete-like locomotion mode to generate a series of undulatory gaits over different kinds of unstructured terrain, which is congruent with the locomotion abilities exhibited by its biological counterpart. Ideally, such an undulatory prototype would allow the implementation of both polychaete-like and eel-like undulatory modes, to enable the experimental comparative assessment of the two modes by altering the orientation of the SCM units on the segments’ underside (i.e., mounted transversely or longitudinally with re-

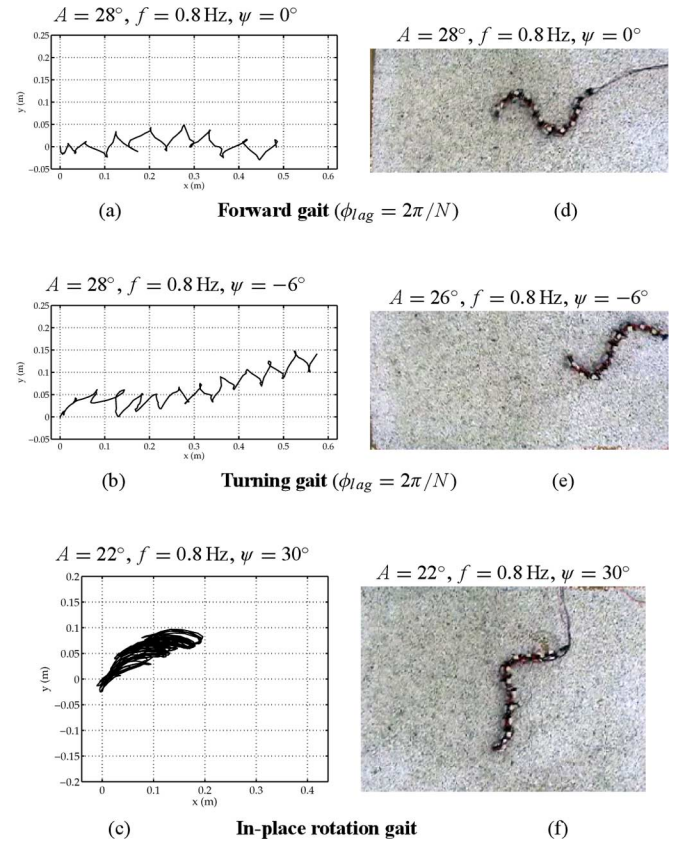


Fig. 16. Experimental results demonstrating polychaete-like undulatory gait generation on *gravel* by the 11-link prototype equipped with single-blade SCMs: (a–c) Representative trajectories of the mechanism’s tail link, (d–f) Image stills. In all instances, the robot initially lies along the x -axis.

spect to the segment axis). However, the friction differential of the current SCM designs is rather small, so that the longitudinal mounting of the single-blade SCM units yields an μ_T/μ_N ratio of about $0.73/0.88 \simeq 1/1.2$ for the robot’s segments. This, according to the simulation results of Section III-B (Coulomb friction), is not expected to suffice for generating eel-like undulatory locomotion. Experiments with the aforementioned configuration of the mechanism verified this prediction of the computational models, as the robot still moved in polychaete-like mode (i.e., along the body wave direction), albeit at a reduced speed, compared to when the SCMs were mounted transversely with respect to the segments. Apart from providing further validation for the computational models employed to analyze the behavior of the system, these findings highlight that alternative SCM designs, characterized by a higher friction differential, are required to explore experimentally both eel-like and polychaete-like undulatory modes over unstructured substrates. For motion over smooth hard surfaces, the use of wheels (as in “classical” undulatory locomotors) provides such a friction differential. We have, in fact, been able to generate both eel-like and polychaete-like gaits with the undulatory prototype of [8], by the longitudinal and transversal, respectively, mounting of wheel modules on the underside of the mechanism’s segments.

Finally, it is worth mentioning that the experimental findings of this paper, most notably the generation of undulatory gaits by tail-to-head body waves and the close agreement of experimental and simulation results, were replicated also with a different robot morphology, namely that of the five-segment pedundulatory prototype of [18].

VII. CONCLUSION

This paper initiates the study of a class of biomimetic robots, which are inspired from the morphology and locomotion of the polychaete annelid worms. The paper focuses on one aspect of such robots, namely the study, both experimental and in simulation, of the locomotion on sand by tail-to-head body undulations. To the best of the authors' knowledge, this is the first work on undulatory robotic locomotion, which demonstrates propulsion and motion control on granular substrates, without the help of wheels or tracks, and considers this novel tail-to-head undulatory mode [17].

Apart from the results presented here, evidence was obtained, during these experiments, that this mode of robotic locomotion performs well on different types of sand, and over a wide range of robot sizes, from the ones presented here to robots whose size is one order of magnitude less [26].

Future work will explore further this mode of locomotion on additional unstructured substrates (e.g., mud), the engineering of more effective ways for the frictional interaction with the environment, the coupling of body undulations with parapodia [18], and the use of sensory information in closed-loop motion control schemes [7], [8].

ACKNOWLEDGMENT

The authors thank the members of the CVRL group of ICS-FORTH, and G. Orlandi, A. Moglia, and O. Tonet for their technical assistance, as well as the members of the BI-OLOCH consortium for their contributions. D. P. T. thanks P. S. Krishnaprasad for insightful discussions.

REFERENCES

- [1] J. Ayers, *Neurotechnology for Biomimetic Robots*, J. L. Davis and A. Rudolph, Eds. Cambridge, MA: MIT Press, 2003.
- [2] S. Hirose, *Biologically Inspired Robots: Snake-Like Locomotors and Manipulators*. New York: Oxford University Press, 1993.
- [3] G. Orlovsky, T. Deliagina, and S. Grillner, *Neuronal Control of Locomotion: From Mollusc to Man*. Oxford, U.K.: Oxford University Press, 1999.
- [4] M. Dickinson, C. Farley, R. Full, M. Koehl, R. Kram, and S. Lehman, "How animals move: An integrative view," *Science*, vol. 288, no. 5463, pp. 100–106, 2000.
- [5] A. Menciassi and P. Dario, "Bio-inspired solutions for locomotion in the gastrointestinal tract: Background and perspectives," *Philos. Trans. R. Soc. Lond. A, Math. Phys. Sci.*, vol. 361, pp. 2287–2298, 2003.
- [6] A. Menciassi, S. Gorini, G. Pernorio, and P. Dario, "A SMA actuated artificial earthworm," in *Proc. IEEE Int. Conf. Robot. Autom.*, New Orleans, LA, 2004, pp. 3282–3287.
- [7] M. Sfakiotakis and D. P. Tsakiris, "Neuromuscular control of reactive behaviors for undulatory robots," *Neurocomputing*, vol. 70, no. 10–12, pp. 1907–1913, 2007.
- [8] M. Sfakiotakis and D. P. Tsakiris, "A biomimetic centering behavior for undulatory robots," *Int. J. Robot. Res.*, vol. 26, no. 11–12, pp. 1267–1282, pp. 2007.
- [9] J. Lighthill, *Mathematical Biofluidynamics*. Philadelphia, PA: SIAM, 1975.
- [10] S. Hirose and E. Fukushima, "Snakes and strings: New robotic components for rescue operations," *Int. J. Robot. Res.*, vol. 23, no. 4–5, pp. 341–349, 2004.
- [11] J. P. Ostrowski and J. Burdick, "The geometric mechanics of undulatory robotic locomotion," *Int. J. Robot. Res.*, vol. 17, no. 7, pp. 683–701, 1998.
- [12] P. S. Krishnaprasad and D. P. Tsakiris, "Oscillations, SE(2)-snakes and motion control: A study of the roller racer," *Dyn. Syst.*, vol. 16, no. 4, pp. 347–397, 2001.
- [13] S. Ma, "Analysis of creeping locomotion of a snake-like robot," *Adv. Robot.*, vol. 15, no. 2, pp. 205–224, 2001.
- [14] M. Saito, M. Fukaya, and T. Iwasaki, "Modeling, analysis, and synthesis of serpentine locomotion with a multilink robotic snake," *IEEE Control Syst. Mag.*, vol. 22, no. 1, pp. 64–81, Jan. 2002.
- [15] M. Nilsson, "Serpentine locomotion on surfaces with uniform friction," in *Proc. IEEE/RSJ Int. Conf. Intell. Robots Syst.*, Sendai, Japan, 2004, pp. 1751–1755.
- [16] K. A. McIsaac and J. P. Ostrowski, "Experimental verification of open-loop control for an underwater eel-like robot," *Int. J. Robot. Res.*, vol. 21, pp. 849–860, 2002.
- [17] D. P. Tsakiris, M. Sfakiotakis, A. Menciassi, G. La Spina, and P. Dario, "Polychaete-like undulatory robotic locomotion," in *Proc. IEEE Int. Conf. Robot. Autom.*, Barcelona, Spain, 2005, pp. 3029–3034.
- [18] M. Sfakiotakis, D. P. Tsakiris, and K. Karakasiliotis, "Polychaete-like pedundulatory robotic locomotion," in *Proc. IEEE Int. Conf. Robot. Autom.*, Roma, Italy, 2007, pp. 269–274.
- [19] P. Dewit. (2007). [Online]. Available: <http://www.flickr.com/photos/peterdewit/>
- [20] J. Gray, "Studies in animal locomotion. VIII. The kinetics of locomotion of *Nereis diversicolor*," *J. Exp. Biol.*, vol. 16, pp. 9–16, 1939.
- [21] R. Brusca and G. Brusca, *Invertebrates*. Sunderland, U.K.: Sinauer Associates, 1990.
- [22] R. B. Clark, "Undulatory swimming in polychaetes," in *Perspect. Exp. Biol., Proc. 15th Anniversary Meeting Soc. Exp. Biol.*, P. Davis, Ed. New York: Pergamon, 1976, vol. 1, pp. 437–446.
- [23] R. B. Clark and M. E. Clark, "The ligamentary system and segmental musculature of *Nephtys*," *Quart. J. Micr. Sci.*, vol. s3-101, no. 2, pp. 149–176, 1960.
- [24] T. Hesselberg, "Biomimetics and the case of the remarkable ragworms," *Naturwissenschaften*, vol. 94, no. 8, pp. 613–621, 2007.
- [25] G. La Spina, T. Hesselberg, J. Williams, and J. Vincent, "A biomimetic approach to robot locomotion in unstructured and slippery environments," *J. Bion. Eng.*, vol. 2, pp. 1–14, 2005.
- [26] N. Ng Pak, S. Scapellato, G. La Spina, G. Pernorio, A. Menciassi, and P. Dario, "Biomimetic design of a polychaete robot using IPMC actuator," in *Proc. 1st IEEE/RAS-EMBS Int. Conf. Biomed. Robot. Biomechatron. (BIOROB'06)*, Pisa, Italy, pp. 666–671.
- [27] M. Sfakiotakis and D. P. Tsakiris, "SIMUUN: A simulation environment for undulatory locomotion," *Int. J. Model. Simul.*, vol. 26, no. 4, pp. 4430–4464, 2006.
- [28] A. M. Bloch, P. S. Krishnaprasad, J. E. Marsden, and R. M. Murray, "Non-holonomic mechanical systems with symmetry," *Arch. Ration. Mech. Anal.*, vol. 136, no. 1, pp. 21–99, 1996.
- [29] J. Cortes, S. Martinez, J. P. Ostrowski, and K. A. McIsaac, "Optimal gaits for dynamic robotic locomotion," *Int. J. Robot. Res.*, vol. 20, no. 9, pp. 707–728, 2001.
- [30] J. Marsden and T. Ratiu, *Introduction to Mechanics and Symmetry*. New York: Springer-Verlag, 1994.
- [31] A. Bloch, *Nonholonomic Mechanics and Control*. New York: Springer-Verlag, 2003.
- [32] R. M. Murray, "Nonlinear control of mechanical systems: A Lagrangian perspective," *Annu. Rev. Control*, vol. 21, pp. 31–42, 1997.
- [33] G. Taylor, "Analysis of the swimming of long and narrow animals," *Proc. R. Soc. Lond. A, Math. Phys. Sci.*, vol. 214, pp. 158–183, 1952.
- [34] Ö. Ekeberg, "A combined neuronal and mechanical model of fish swimming," *Biol. Cybern.*, vol. 69, no. 5–6, pp. 363–374, 1993.
- [35] A. J. Ijspeert, "A connectionist central pattern generator for the aquatic and terrestrial gaits of a simulated salamander," *Biol. Cybern.*, vol. 85, no. 5, pp. 331–348, 2001.
- [36] M. E. J. Holwill and M. A. Sleight, "Propulsion by hispid flagella," *J. Exp. Biol.*, vol. 47, no. 2, pp. 267–276, 1967.
- [37] J. Gray and G. J. Hancock, "The propulsion of sea-urchin spermatozoa," *J. Exp. Biol.*, vol. 32, no. 4, pp. 802–814, 1955.

- [38] M. C. Lagomarsino, F. Capuani, and C. P. Lowe, "A simulation study of the dynamics of a driven filament in an Aristotelian fluid," *J. Theor. Biol.*, vol. 224, pp. 215–224, 2003.
- [39] L. Fauci, "A computational model of the fluid dynamics of undulatory and flagellar swimming," *Am. Zool.*, vol. 36, no. 6, pp. 599–607, 1996.
- [40] H. Olsson, K. Åström, C. de Wit, M. Gäfvert, and P. Lischinsky, "Friction models and friction compensation," *Eur. J. Control*, vol. 29, no. 4, pp. 176–195, 1998.
- [41] G. Gabrielli and T. H. von Karman, "What price speed?" *Mech. Eng.*, vol. 72, pp. 775–781, 1950.



Giovanni La Spina received the Laurea degree (110/110) in mechanical engineering (biomedical) from the University of Pisa, Italy, in 2000, and the Ph.D. degree (100/100 *cum laude*) in biomedical engineering from the Scuola Superiore S. Anna, Pisa, in 2005.

He has collaborated in scientific projects, at the European level, in the field of Biomimetics. In particular, from 2002 to 2005, he worked on an European Project "BIOmimetic structure for LOComotion in Human body (BioloCh)". He is currently working as a Postdoctoral Research Fellow at the Center for Research in Microengineering (CRIM) Laboratory, Scuola Superiore S. Anna—PSV Pontedera (PI), Pisa. His current research interests include the fields of computer graphics and animation, biomimetics, bio-inspired robotics, and microfabrication technologies.



Michael Sfakiotakis received the B.S. degree in electrical engineering from the Aristotle University of Thessaloniki, Thessaloniki, Greece, in 1995, the M.Sc. degree in communications, control, and digital signal processing (DSP) from Strathclyde University, Glasgow, U.K., in 1996, and the Ph.D. degree in electrical engineering from Heriot-Watt University, Edinburgh, U.K., in 2000.

Since 2002, he is a Research Associate at the Institute of Computer Science, Foundation for Research and Technology—Hellas (FORTH), Heraklion, Greece. His current research interests include the areas of biologically inspired robotics, locomotion control, and systems modeling.

Dr. Sfakiotakis is a member of the Technical Chamber of Greece.



Dimitris P. Tsakiris (S'86–M'95) received the B.S. degree from the National Technical University of Athens, Greece, in 1986, and the M.S. and Ph.D. degrees from the University of Maryland, College Park, in 1988 and 1995, respectively, all in electrical engineering.

From 1995 to 1998, he was a Marie Curie Postdoctoral Fellow at the Institut National de Recherche en Informatique et en Automatique (INRIA), Sophia-Antipolis, France. Since 1999, he has been with the Institute of Computer Science, Foundation

for Research and Technology—Hellas (FORTH), Heraklion, Greece, where he is currently a Principal Researcher. He is also a Faculty Member of the Graduate Program in the Brain and Mind Sciences, and a Visiting Professor with the Departments of Computer Science and Applied Mathematics at the Uni-

versity of Crete, Heraklion. He is a Principal Investigator and Co-Investigator of several European IST projects related to his research interests. He is also a Project Proposal Evaluator for the EU IST Program. His current research interests include the areas of robotics, nonlinear control, geometric mechanics, and computational vision, in particular, biologically inspired approaches to robotic locomotion, control, and sensing.

Dr. Tsakiris is a member of the Technical Chamber of Greece. He has served as a Program Committee Member and Reviewer for several IEEE conferences and publications.



Arianna Menciassi (M'02) received the Laurea degree (with Honors) in physics from the University of Pisa, Pisa, Italy, in 1995, and the Ph.D. degree in bioengineering from the Center for Research in Microengineering (CRIM) Laboratory, Scuola Superiore Sant'Anna, Pisa, in 1999.

Since June 2006, she is an Associate Professor of Biomedical Robotics at the Scuola Superiore Sant'Anna. She teaches and supervises several Masters and Ph.D. students at the CRIM Laboratory. She is working on several European projects and international projects for the development of micro- and nanorobotic systems (often bioinspired) for medical applications. She is the author or coauthor of more than 90 papers published in international journals, 40 of these in ISI journals. She is the holder of several international and national patents. Her current research interests include the fields of biomedical, micro- and nanorobotics, biorobotics, microsystem technologies, nanotechnologies, and micromechatronics.

Dr. Menciassi was the recipient of the Best Manipulation Paper Award at the International Conference on Robotics and Automation in 2001.



Paolo Dario (M'88–SM'01–F'03) received the Dr. Eng. degree in mechanical engineering from the University of Pisa, Pisa, Italy, in 1977.

He is currently a Professor of Biomedical Robotics at the Scuola Superiore Sant'Anna, Pisa. He also teaches at the School of Engineering, University of Pisa. He has been a Visiting Professor at many universities, including Brown University, Providence, RI, the Ecole Polytechnique Federale de Lausanne (EPFL), Lausanne, Switzerland, Waseda University, Tokyo, Japan, College de France, Paris, France, Ecole Normale Supérieure de Cachan, Cachan, France, and Zhejiang University, Zhejiang, China. He was the founder of the Advanced Robotics Technologies and Systems (ARTS) Laboratory and is currently the Co-Cordinator of the Center for Research in Microengineering (CRIM) Laboratory, Scuola Superiore Sant'Anna, where he supervises a team of about 70 researchers and Ph.D. students. He is also the Director of the Polo Sant'Anna Valdera, the Science Park of the Scuola Superiore Sant'Anna. He is the Coordinator of many national and European projects, and is the Editor-in-Chief, Associate Editor, and Member of the Editorial Board of many international journals. He is the author or coauthor of more than 200 papers published in international journals, 140 of them in ISI journals, and is the Editor of two books in Robotics. His current research interests include the fields of biorobotics, medical robotics, mechatronics, and micro/nanoengineering.

Prof. Dario is a Fellow of the European Society on Medical and Biological Engineering. He is a member of the Board of the International Foundation of Robotics Research (IFRR). He served as the President of the IEEE Robotics and Automation Society during 2002–2003. He was the recipient of many honors and awards, such as the Joseph Engelberger Award.